



HAL
open science

Accuracy of Heat Load Transfer in a Quasi-Dynamic Fluid-Structure Interaction

Rocco Moretti, Marc Lazareff, Marc Errera, Frédéric Feyel, Tristan Soubrié,
Farid Benyoucef

► **To cite this version:**

Rocco Moretti, Marc Lazareff, Marc Errera, Frédéric Feyel, Tristan Soubrié, et al.. Accuracy of Heat Load Transfer in a Quasi-Dynamic Fluid-Structure Interaction. 2019. hal-02262368

HAL Id: hal-02262368

<https://hal.science/hal-02262368>

Preprint submitted on 2 Aug 2019

HAL is a multi-disciplinary open access archive for the deposit and dissemination of scientific research documents, whether they are published or not. The documents may come from teaching and research institutions in France or abroad, or from public or private research centers.

L'archive ouverte pluridisciplinaire **HAL**, est destinée au dépôt et à la diffusion de documents scientifiques de niveau recherche, publiés ou non, émanant des établissements d'enseignement et de recherche français ou étrangers, des laboratoires publics ou privés.

Accuracy of Heat Load Transfer in a Quasi-Dynamic Fluid-Structure Interaction

Rocco Moretti^{a,b}, Marc Lazareff^a, Marc Errera^a, Frédéric Feyel^c, Tristan Soubrié^d, Farid Benyoucef^e

^a*DAAA, ONERA, Université Paris-Saclay, 29 Avenue de la Division Leclerc, F-92320 Châtillon, France*

^b*Centre des Matériaux - Mines Paristech, 63 - 65 rue Henri-Auguste Desbrueres, F-91003 Évry cedex, France*

^c*SafranTech, Safran Group, Rue des Jeunes Bois, Châteaufort, F-78772 Magny-les-Hameaux Cedex, France*

^d*Andheo, F-92322 Châtillon Cedex, France*

^e*SAFRAN Aircraft Engines, site de Villaroche, Rond-Point René Ravaud - F-77550 Moissy Cramayel, France*

Abstract

This paper is devoted to investigate the temporal and spatial accuracy in transient conjugate heat transfer problems where the influence of unsteadiness in the fluid is supposed to be negligible. The numerical method is based on an iterative procedure with interpolated boundary conditions on the solid side. Emphasis is put on these interpolation procedures. First it is shown that a temporal interpolation is by no means the most appropriate way of estimating the flow boundary conditions prescribed on the coupled solid surfaces. In contrast, when these conditions are based on the heat flux/temperature linearity, significantly better results are obtained. Indeed, they compare very well against a reference solution provided by a non-iterative and non-interpolated coupled computation. Moreover, important improvements were made by adequately defining the integral contribution of the boundary condition using the Gauss points in the finite element solid code. Finally, it was also revealed that a relevant approximation of the heat transfer requires a sufficiently fine solid mesh at the interface.

Keywords: Transient CHT, Interpolation methods, Thermal interaction,

Email address: rocco.moretti@onera.fr (Rocco Moretti)

Nomenclature

Acronyms

BC	Boundary Condition
CHT	Conjugate Heat Transfer
FEM	Finite Element Method
FVM	Finite Volume Method
MTO	Maximum take-off
NS	Navier-Stokes
RANS	Reynolds-Averaged Navier-Stokes

Physics Constants

α	coupling coefficient	$W/(m^2K)$
Bi^Δ	mesh Biot number	
Δt	time step	s
Δy	first cell size	m
F	inviscid and viscous flux	
D	Fourier number	
$inter_y(x)$	linear interpolation with respect to y of x	
κ	thermal conductivity	$W/(mK)$
\mathbf{K}	thermal conductivity matrix	$W/(mK)$
Ω	physical domain	

ρc_p	volumetric heat capacity	$J/(Km^3)$
ρ	density	kg/m^3
Γ	coupled interface	
\mathbf{v}	inward-pointing unit normal	
\mathbf{w}	conservative quantity vector	
a_s	thermal diffusivity	m^2/s
c_p	the specific heat capacity at constant pressure	$J/(kgK)$
h	heat transfer coefficient	$W/(m^2K)$
K	thermal conductance	$W/(m^2K)$
L	solid characteristic length	m
Q	generic quantity	
q	heat flux	W/m^2
T	temperature	K
t	time	s
T_{ref}	reference temperature (here it is the fluid inlet temperature)	K
U	fluid velocity	m/s
y^+	Dimensionless wall distance	

Subscripts

∞	far from the interface (fluid inlet)
c	coupled
f	fluid
k	solid subiterations between two coupling times
s	solid

Superscripts

- $\hat{}$ variable to compute
- n coupling iteration (counting the number of steps in the iterative process)

1. Introduction

Accurate prediction of aero-engine metal heat conduction is of paramount importance in the engine process in general and in high pressure turbine heat transfer designs in particular. Indeed, the temperature field throughout the solid material is an essential factor exerting a great influence on the induced thermal stress, material properties, and fatigue-creep (Sun et al. (2012); Amirante et al. (2012); Rezazadeh Reyhani et al. (2013); Mukherji et al. (2015)).

The transient component metal temperature is the result of internal/external convective heat transfer and the time-dependent conduction through the solid itself. Therefore, an interaction model between the fluid and the solid media is required. The term conjugate heat transfer (CHT) is used when the two modes of heat transfer - convection and conduction - are considered simultaneously, Perelman (1961). CHT procedures are now commonly found in many real-world environments in which accurate heat transfer predictions are needed.

Only fully conjugate heat transfer computations allow correct analysis of heat and mass transfer. However, a numerical treatment of a transient process in both media would lead to accurate but excessively expensive simulations in terms of CPU time and would provide information far beyond what is needed for engineering analysis and design.

The time-accurate prediction of CHT problems can be computationally expensive, although significant progress has been achieved in this area. Its application has been mainly limited to steady simulations for many years, specifically when a two-way coupling method is required, i.e. whenever the physical coupling between the fluid and solid models involves significant interactions. It is the reason why its application remains limited to steady or simple transient simulations and has not become a current design tool in industry. Nevertheless increased attention is being devoted to transient issues during specific periods of an engine cycle (start up, shutdown, cruise) to obtain precise thermal behavior.

In a transient aero-engine flight cycle, the solid computations in the fluid-solid coupling must be unsteady in order to obtain a detailed local knowledge of the slow response of metal heat conduction to changes in operating conditions. On the other hand, the fluid flow time scales are much shorter, as the ratio between the solid and the fluid time scales can be up to 10^4 for gas turbine blades (He and Oldfield (2009)). As a result, one may reasonably assume that the influence of unsteadiness is negligible on the fluid side (Sun et al. (2008); Ganine et al. (2012); Errera and Baqué (2013); Baque et al. (2013); Gimenez et al. (2016)). Note that other interesting alternative approaches can be designed (He and Fadl (2017)).

Two major challenges to the improvement of CHT predictions are stability and accuracy.

Regarding the first issue, CHT studies have so far been very much oriented to stability issues and to having the right conditions at the fluid-solid interface in a partitioned approach. Indeed, partitioned approaches are very popular and largely used in aeroelastic problems, but they suffer from stability limitations due to the fact that the fluid and solid interfaces are solved separately (Felippa and Park (1980); Piperno et al. (1995)). Partitioned methods are also largely employed in CHT (see for example Kuntz et al. (2001); Liu et al. (2005)). It is the reason why, in recent years, the behavior (well-posedness, stability, convergence) of interface conditions in a CHT partitioned procedure techniques has been addressed in different ways such as a normal mode analysis (Roe et al. (2008); Henshaw and Chand (2009); Kazemi-Kamyab et al. (2014); Joshi and Leyland (2014); Verstraete and Scholl (2016)) or the energy method (Lindström and Nordström (2010)). However, in most existing stability studies, the focus is primarily on steady regimes.

A stability analysis for thermally coupled fluid-structure problems in a quasi-dynamic regime was presented by Errera et al. (2017). This mathematical investigation provided relevant interface conditions, obtained from a simplified model problem and it has been shown that fast and accurate prediction of solid temperature can be obtained in a wide range of fluid-solid interaction regimes, i.e. from low to very large Biot numbers. For instance, it is often noted in the literature that realistic CHT computations are prone to oscillations that can ultimately lead to a divergent process. It is then essential to note here that the interfacial schemes proposed by ONERA, namely the so-called optimal coupling coefficients presented for the first time by Errera and Chemin (2013) lead to fast converging solutions in any case, either in

steady (Errera and Duchaine (2016); El Khoury et al. (2017); Moretti et al. (2018)) or unsteady (Errera and Turpin (2013); Errera et al. (2017)) CHT.

Once the stability problems are dealt with efficiently and appropriately strategy, accuracy issues can be considered. In a quasi-dynamic approach, in order to bridge the disparity in time scales between convection and solid conduction during a long-time period, a sequence of fluid steady states is considered. Two coupling times define a ramp and the whole cycle is composed of 10-20 ramps at the most. In a given ramp, accurate solutions are obtained from the thermal coupling at each ramp-defining point in time. Whereas at each temporal solid step, in between the coupling times, boundary conditions are estimated generally via a linear temporal interpolation. However, linear time-dependent operating conditions may be considered *a priori* as unfounded and thus may prove to be unreliable. This fundamental aspect will be discussed hereafter.

This paper is devoted entirely to the investigation of the temporal and spatial accuracy in quasi-dynamic CHT coupling processes, with emphasis put on interpolation procedures. In order to evaluate precisely the performances of these procedures, a full coupling process will be carried out. This is a process where the thermal coupling is carried out systematically, at each temporal solid state. It is well understood that full coupling process is particularly expensive and must be prohibited in realistic problems. On the other hand, a full coupling process contains no interpolation. As a result, it can be seen as a "reference solution", i.e. a comprehensive and efficient solution to identify and measure the most accurate interpolation procedure. Other "accuracy issues" are addressed in this paper, namely the fluid-solid interface treatment. In this regard, some relevant papers are already available to deal with the effect of non-matching meshes (Jaiman et al. (2006)) or to get a conservative schemes (Jiao and Heath (2004); Jaiman et al. (2005)). However, another aspect will be addressed here. Emphasis will be put on the exchange of data between a finite-volume fluid solver and a finite-element solid solver and a practical means to obtain an accurate fluid-solid solution, independent of the interfacial treatment, will be provided.

2. Numerical Methods

2.1. Finite volume fluid solver

The governing equations for compressible flow are the Navier-Stokes (NS) equations that can be written in the form:

$$\frac{\partial \mathbf{w}_f}{\partial t} + \nabla \cdot [F(\mathbf{w}_f)] = 0 \quad \text{in } \Omega_f \quad (1)$$

where \mathbf{w}_f represents the vector of mass, momentum and energy density, F represents the flux including inviscid and viscous terms. The Navier-Stokes (NS) equations are discretized with the Finite Volume Method (FVM). The inviscid terms are solved using a second-order upwind spatial discretization. The viscous terms are discretized with a five-point central difference formulation. The time integration is obtained by an implicit method.

2.2. Finite element solid solver

In the solid domain, Ω_s , the temperature is solved using the heat equation. The heat equation is a parabolic partial differential equation that describes the distribution of heat (or variation in temperature) in a given region over time. If there are no heat sources, the heat equation is:

$$\rho c_p \frac{\partial \mathbf{T}}{\partial t} - \nabla \cdot (\mathbf{K} \cdot \nabla \mathbf{T}) = 0 \quad \text{in } \Omega_s \quad (2)$$

where $\mathbf{T} = T(x, y, z, t)$ is the unknown temperature field, \mathbf{K} is the thermal conductivity matrix, ρ is the density and c_p is the specific heat capacity at constant pressure. The product ρc_p is the volumetric heat capacity.

2.3. Example of a transient cycle

The aim of this study is to improve the accuracy of a two-way coupling procedure for practical CHT applications during a full transient flight cycle. This cycle is above all characterized by a long period of time, that is, the entire duration of a flight (i.e. several hours). This is needed since high requirements about the life-span of the engine elements are required, in particular heat load characteristics during all the stages of a flight. These stages are expressed by ramps and these ramps are defined from ramp points, namely specific instants representing changes in operating conditions.

Figure 1 gives an example of a transient cycle where a typical quantity Q (engine speed, temperature, flow rate, ...) is plotted over time. One can

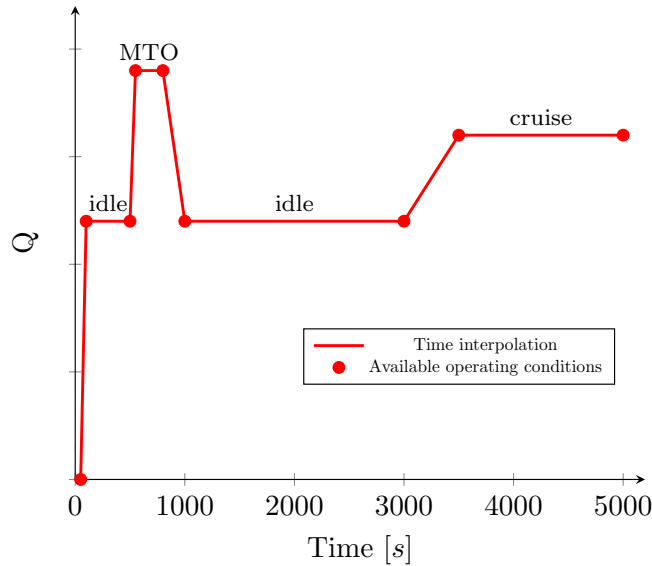


Figure 1: Example of a transient cycle

see that this cycle covers a broad range of usual operating conditions from stand-still, idle, engine acceleration to maximum take-off (MTO), and cruise conditions. The time intervals, also simply called “ramps”, are pre-established instants from the time position of ramp points where environment conditions are available. In these ramps, linear distributions of the environment parameters are assumed. It is only at ramp points that a fluid-structure coupling may take place without further hypothesis. These points can also be regarded as coupling times. Outside these specific and limited instants, flow conditions are not known and must be interpolated. In contrast, there are no restrictions on the number of solid time steps. In other words, each ramp can be subdivided into as many temporal divisions as are required to analyze the transient heat conduction in solid regions.

2.4. Time scale disparities

A transient coupling process is challenging due to the great time-scale disparities of the physical model between the fluid and the solid. The fluid flow requires usually a much smaller temporal resolution than the structure. Accordingly, a description of transients in the fluid would be almost impractical over a period comparable to the thermal response time of the solid. It is then necessary to develop simplified coupling strategies to minimize the

number of CFD runs.

2.5. A quasi-dynamic strong approach

An interesting coupling procedure is used to limit the computational cost due to the CFD. Because the resolution of the fluid transient is not sought, this procedure considers the flow solution as a sequence of steady states. In most cases, this assumption is valid since the solid and the fluid operate on different time constants, and consequently, the influence of the unsteadiness of the fluid is negligible. In summary, this procedure couples the solid resolution in time with a sequence of fluid steady states. This approach has been called "quasi-dynamic" or "quasi-steady assumption" to highlight the partial resolution of the system transient.

In general, in steady CHT problems the equilibrium of the fluid-solid interface is not enforced during the computation, but only when convergence has been reached (weak coupling). However Koren et al. (2017) showed that using a hybrid Dirichlet-Dirichlet method and solving each domain with a conservative numerical scheme, the energy conservation through the medium interface is ensured. In the case of transient CHT problems, the solution evolves over time, i.e. it depends on the solution at the previous physical time step. Thus, the interface equilibrium has to be enforced at every physical time step which corresponds to a strong coupling approach. Strong coupling can be achieved with monolithic procedures where fluid and solid domains are solved simultaneously ensuring the conservativity at the interface. This can be very time consuming when the physical time period to compute is large. Furthermore, it often leads to ill-conditioned systems as Farhat and Lesoinne (2000) explain. The second family of coupling methods are the partitioned procedures. They were developed in order to speed up the coupling computations using different time steps for each physical problem. Unfortunately, these methods are weak coupling approaches by definition. As a result, appropriate adjustments are required to convert them into strong coupling approaches in order to carry out transient coupling computation. A sub-iteration process is set up at every coupling time to reach a converged solution verifying the equilibrium of the fluid-structure interface.

Figure 2 shows the "quasi-dynamic strong algorithm" used in the present paper:

- 1 Transient calculation in the solid from t_c to $t_c + \Delta t_c$
- 2 Exchange from the solid to the fluid

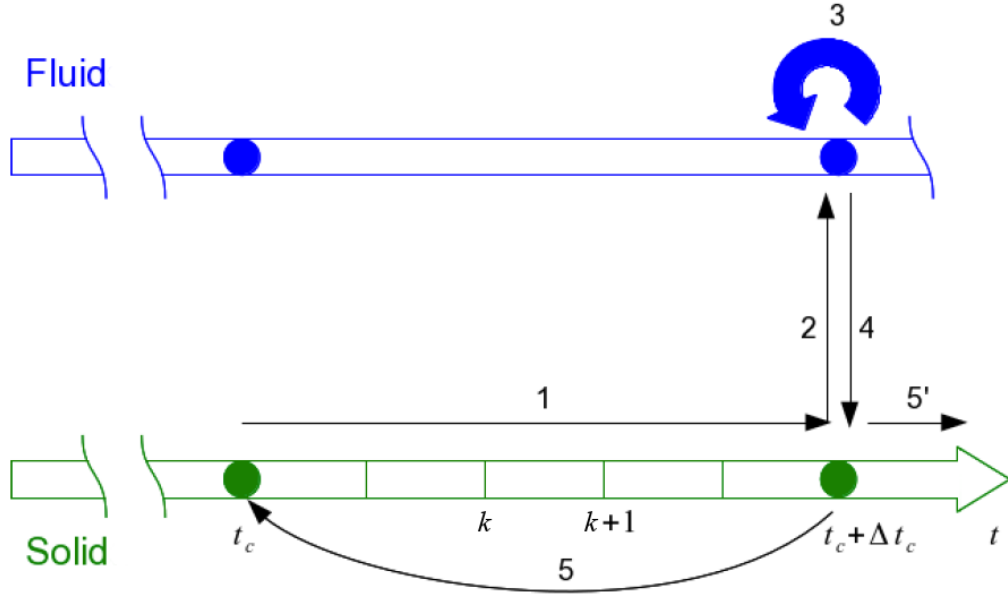


Figure 2: The "quasi-dynamic" strong algorithm

- 3 Steady fluid computation at time $t_c + \Delta t_c$
- 4 Exchange from the fluid to the solid

Convergence Test: Comparison between solid and fluid at the interface at time $t_c + \Delta t_c$. Converged?

- 5 No: Go back to time t_c and remake steps 1-4 until convergence.
- 5' Yes: transient computation until time $t_c + \Delta t_c$ is achieved. Advance over time to the next coupling time.

Fluid states are known only at a few physical times, therefore interpolated fluid states have to be used as boundary conditions at every temporal solid increment to advance the solid resolution in time (step 1 in Fig. 2). The present paper focuses on this aspect.

Hereinafter, the set of steps 1-4, as well as the convergence test, will be called *coupling iteration*.

2.6. Fluid solid interface condition

This paper will not focus on the stability of the coupling method; only the common Dirichlet-Robin interface condition will be used. This condition, widely used in the literature, consists of imposing a temperature profile (Dirichlet condition) on the fluid solver and the Robin condition on the solid one.

The Robin condition is a linear relationship between the temperature and the heat flux. At the fluid-solid interface, a general Robin condition on the solid side during the coupled resolution leads to the equation:

$$\hat{q}_s + \alpha_f \hat{T}_s = -q_f + \alpha_f T_f \quad (3)$$

where q is the normal heat flux, T is the temperature and α is a coupling coefficient, the super-imposed hat symbol ($\hat{}$) denotes the sought values. Note that $q_s = -K_s \partial T_s / \partial \mathbf{v}_s$ and $q_f = -K_f \partial T_f / \partial \mathbf{v}_f$ are the normal solid and fluid heat flux respectively (\mathbf{v} is inward-pointing unit normal) where K is the thermal conductance. The definition of the thermal conductances are $K_f = \kappa_f / (\nu \Delta y_f)$ ($\nu = 1/2$ if FVM or $\nu = 1$ if FEM) and $K_s = \kappa_s / \Delta y_s$ where Δy_f and Δy_s are respectively the size of fluid and solid cell adjacent to the coupled interface.

It is an interesting boundary condition meant to stabilize and accelerate the convergence of fluid-structure coupling problems. As Errera et al. (2017) have shown, it is possible to stabilize and obtain the best convergence speed using appropriate coupling coefficients α_f .

At convergence, the Robin condition ensures the continuity of temperature and heat flux at the interface, i.e. the solution should be independent of the coupling coefficient. This is one of the criteria a correct coupling algorithm must satisfy. Often it is not the case, as the test case in Section 3 will illustrate.

2.7. Reminder on the interfacial fluid-solid schemes

This paper is not devoted to implement stable conditions at the fluid-solid interface. These conditions have been already described precisely elsewhere. Moreover, in order to highlight the loss of precision and the coupling coefficient-dependency, extreme conditions will be implemented (very high values of the coupling coefficients - far from optimal!). However, in this paper, when an efficient solution is sought, optimal coefficients (in terms of convergence and CPU time) will be used.

For the sake of clarity and coherence, this section briefly summarizes the main results of the stability analysis and provides the mathematical expression of the main relevant adaptive coefficients in a quasi-dynamic approach. The reader is referred to Errera et al. (2017) for a more complete presentation.

In CHT analysis, adaptive coefficients have been expressed for the first time in Errera and Chemin (2013). They are derived from a normal mode stability analysis based on the theory of Godunov-Ryabenkii. However, this study was initially devoted to steady CHT solutions only, whereas steady and unsteady CHT have very little in common, Errera and Turpin (2013). Thus, a new stability analysis, specifically dedicated to transient CHT, was carried out.

The main characteristics of the Dirichlet-Robin interface conditions are summarized in Table 1 where the domain and range of $|g|$ (temporal amplification factor of the transient coupled problem) are provided. The conditions both depend upon the mesh Biot number and the mesh Fourier number.

α_f	0		α_f^{min}		$\alpha_f^{(opt)}$		∞	Condition
$ g $		UNSTABLE	1	\searrow	g^{opt}	\nearrow	1	$Bi^\Delta \geq (1 + \overline{D}_s)$
$ g $	g_1^0			\searrow	g^{opt}	\nearrow	1	$(1 + \overline{D}_s)/2 \leq Bi^\Delta \leq (1 + \overline{D}_s)$
$ g $	g_2^0			\searrow			1	$Bi^\Delta \leq (1 + \overline{D}_s)/2$
$\alpha_f^{min} = \frac{h}{2} - \frac{K_s}{2} (1 + \overline{D}_s)$ $\alpha_f^{(opt)} = h - K_s \frac{(1 + \overline{D}_s)}{2}$ $g_1^0 = Bi^\Delta - \overline{D}_s$ $g_2^0 = 1 - Bi^\Delta$ $g^{opt} = \frac{(1 - \overline{D}_s)}{(1 - \overline{D}_s) + 2Bi^\Delta}$								

Table 1: Dirichlet-Robin procedure for transient analysis.
Stability conditions in terms of α_f

The Fourier number is the ratio of diffusive transport rate to the heat storage rate:

$$D_s = \frac{a_s \Delta t_s}{\Delta y_s^2} \quad (4)$$

where a_s is the thermal diffusivity, Δt_s is the solid time step and Δy_s is the solid first cell size in the direction of the surface normal. \overline{D}_s is a normalized Fourier number which varies in the range $[0, 1]$.

The "mesh Biot number" defined by:

$$Bi^\Delta = \frac{h}{K_s} \quad (5)$$

The dimensionless number is used here to characterize the heat transferred from the first solid grid cell to the surrounding fluid.

Table 1 shows the existence of three distinct zones in the numerical behavior of D-R transmission procedure in transient CHT :

1. The first region $[Bi^\Delta > 1 + \overline{D}_s]$ (large mesh Biot number) is characterized by a lower stability limit. In this region, when $\alpha_f > \alpha_f^{min}$, $|g|$ first decreases from 1 to the optimal amplification factor.
2. The second region $[(1 + \overline{D}_s) / 2 < Bi^\Delta < 1 + \overline{D}_s]$ does not exhibit any stability restriction. It is a narrow region where as previously, $|g|$ has an absolute minimum, namely when α_f is equal to the optimal coefficient.
3. The third region $[Bi^\Delta < (1 + \overline{D}_s) / 2]$ (low Biot number) is characterized by a continually increasing function in the domain $\alpha_f \geq 0$. There is no stability restriction. The minimum of the amplification factor is obtained for $\alpha_f = 0$.

At that point, two essential remarks must be made :

- At large Biot numbers, difficult problems, due to non-uniformity of temperature fields within the solid, can arise. This is reflected mathematically by precisely defined stability limits in the case where a temperature is sent to the fluid side (1st row of Table 1). In practice, even if the optimal coefficient is very close to the heat transfer coefficient $\alpha_f \approx h$ (h is the heat transfer coefficient), this choice must be avoided in general. Indeed, Table 1 shows that the stability limit is very close $\alpha_f^{min} \approx h/2$, and this is especially true as the Biot number grows.
- At low Biot numbers, on the contrary, there is no stability limit (2nd and 3rd row of Table 1). This numerical property will enable us in the current paper to study the influence of the coupling coefficient on the accuracy in extreme conditions (very large coefficients), without any stability issues. This is precisely why these regimes will be adopted in this paper.

2.8. Length scale and stability

We are interested in the transient solution in the solid domain and thus in the definition of the conductance, the length of the solid mesh is a natural candidate. However, this choice has adverse effects on stability.

Indeed, it has been shown (Errera et al. (2017)) that for the Dirichlet-Robin condition, the stability bound, at large Biot numbers, is an increasing function of the thermal penetration depth. This is also confirmed by the values given by Table 1. As we can see, the lower stability bound is given by:

$$\alpha_f^{min} = \frac{h}{2} - \frac{K_s}{2} (1 + \overline{D}_s) \quad (6)$$

This means that the CHT computations are theoretically unstable for any coupling coefficient $\alpha_f < \alpha_f^{min}$. In the expression of α_f^{min} , the thermal conductance and the Fourier number are estimated with the solid cell size. Thus, the greater the penetration depth, the greater the value of the stability bound :

$$\alpha_f^{min}(\Delta y_f) < \alpha_f^{min}(2\Delta y_f) < \dots < \alpha_f^{min}(L) \quad (7)$$

where L is a characteristic thickness of the solid domain.

Consequently, the stability limit provided by a given penetration depth can only stabilize phenomena with shorter penetrations but is unstable for higher penetrations. This is a major result obtained by the stability analysis. As a result, the solid thickness must be adopted in the definition of the solid conductance and thus, the numerical Biot number naturally becomes the "traditional" Biot number found in the literature.

At this point, we can adopt the values obtained at steady state, i.e. $\overline{D}_s = 0$ and $K_s^L = \kappa_s/L$. This leads to

$$\alpha_f^{min} = \frac{h}{2} - \frac{K_s^L}{2} \quad (8)$$

that can stabilize the largest penetration depths and has a very little negative impact on the convergence speed. This coefficient provides a highly secure value for the stability bound. This coefficient can also be increased if we adopt $\alpha_f^{min} = \frac{h}{2}$ since it is not easy to define a solid thickness in complex geometries. It is valid at large Biot numbers ($h \gg K_s^L$). At low Biot numbers there is no stability issue, there are no bounds as shown in the 2nd and 3rd row of Table 1.

2.9. Solid interfacial boundary conditions at "non-coupling" instants

As already mentioned, in the "quasi-dynamic" algorithm the transient solid computation is coupled with the steady fluid solution at a few physical times. Between two coupling steps, there is no facing fluid state for every

solid iteration, so these fluid states (blue empty circle in Fig 3) have to be predicted and sent to the solid solver through a "one way coupling". The boundary conditions on the solid are then interpolated between the two fluid states corresponding to the coupling points (blue filled circle in Fig 3).

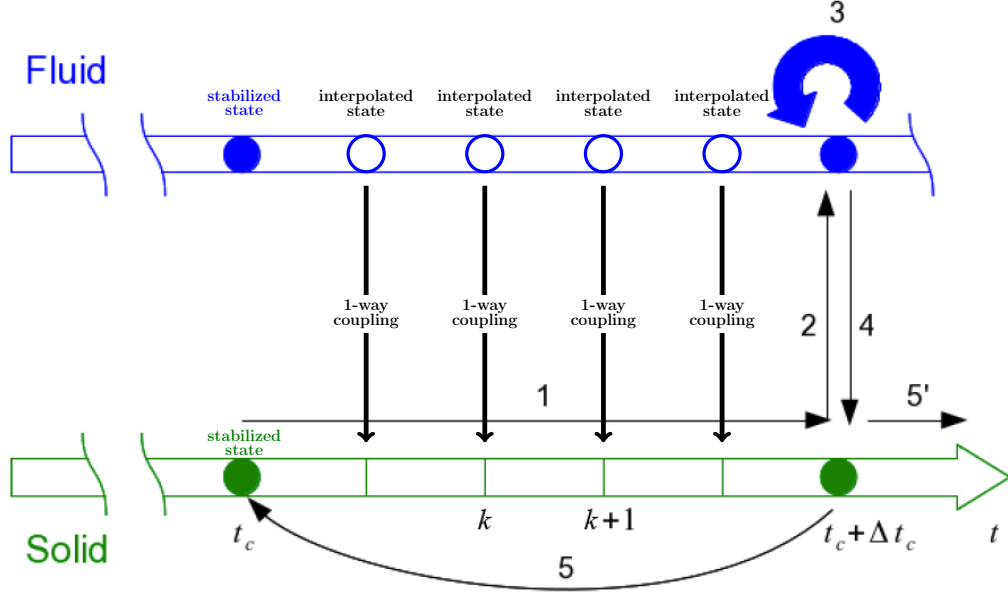


Figure 3: Predicting fluid states for each solid iteration

2.9.1. Linear interpolation in time of both fluid temperature and heat flux (DR1)

Since only two fluid states are available, a linear interpolation in time is the simplest method to use. In the literature, both fluid temperature and heat flux are linearly interpolated in time. In this paper, this method is called *DR1* ("*DR*" stands for Dirichlet-Robin interface condition and "*1*" for method number 1) and it is defined as follows:

$$\begin{cases} \hat{q}_s^n + \alpha_f^{n-1} \hat{T}_s^n = -inter_t(q_f^{n-1}) + \alpha_f^{n-1} inter_t(T_f^{n-1}) & \text{on } \Gamma_s \text{ at } t_k \\ \hat{T}_f^n = T_s^n & \text{on } \Gamma_f \text{ at } t_c \end{cases} \quad (9)$$

where Γ defines the coupled interface and $inter_t(x)$ is the linear interpolation in time of the x quantity such as:

$$x - x_0 = a(t - t_0) \quad \text{with } x_0 = x(t_0), a = const \quad (10)$$

Equation 9 is applied in the fluid only at coupling times because the fluid solution is not considered between two coupling times. Whereas in the solid, Eq. 9 is applied at every solid iteration, including the solid iterations between two coupling times. Practically, the temperature and the heat flux are interpolated at each solid iteration t_k using the extreme values (at t_c and $t_c + \Delta t_c$) computed during the previous coupling iteration $n - 1$. When $n = 1$, a constant prediction is applied.

We want to underline that a linear interpolation is carried out between the initial and the final fluid step at the previous coupling iteration $n - 1$. The initial fluid state does not change within the iterative method because it is already a converged state where the fluid and the solid are in equilibrium. Whereas the final step is updated during every coupling iteration until the fluid-solid equilibrium is reached.

The *DR1* method applies the linear interpolation of the two thermal quantities coming from the fluid, but for specific cases, like a Dirichlet condition on the fluid side, the interpolation of the fluid temperature can be avoided. Indeed, when a Dirichlet condition is used in the fluid solver, this latter receives the solid temperature which is imposed as boundary condition without any transformation. Theoretically, the temperature sent by the solid solver and the temperature it receives after the CFD computation should be the same. Practically, it never happens. The fluid and solid meshes at the interface are usually very different, and the exchanged quantities should be spatially interpolated between the two meshes. In most cases, the spatial interpolation of the Robin condition quantities (combination of heat flux, temperature and the coupling coefficient) is not conservative. Even when matched meshes are used, the error is not nil. Indeed, the fluid domain is usually solved with a Finite Volume Method (FVM), i.e. quantities are computed at the cell center, whereas the Finite Element Method (FEM) is traditionally used in the solid domain, i.e. the system resolution takes place at the cell vertex. The fluid and solid temperatures thus cannot be exactly the same at convergence of the entire coupling problem. Thus, the relaxation term in the Robin equation:

$$\hat{q}_s^n = -inter_t(q_f^{n-1}) + \alpha_f^{n-1} \left(inter_t(T_f^{n-1}) - \hat{T}_s^n \right) \quad \text{on } \Gamma_s \text{ at } t_k \quad (11)$$

does not cancel at convergence. Moreover, if the coupling coefficient α_f^{n-1} is large, the relaxation term could significantly exceed the $inter_t(q_f^{n-1})$ term, resulting in a large dependence of the transient solid problem on the re-

laxation term value. This will be illustrated in section 3 where a strong dependence on the coupling coefficient will be observed.

2.9.2. Linear interpolation in time of just fluid heat flux (DR2)

In the Dirichlet-Robin procedure, the temperature is already available on the solid side and thus can be used directly with no interpolation errors. This modified Dirichlet-Robin interface condition (named *DR2*) can be expressed as:

$$\begin{cases} \hat{q}_s^n + \alpha_f^{n-1} \hat{T}_s^n = -inter_t(q_f^{n-1}) + \alpha_f^{n-1} T_s^{n-1} & \text{on } \Gamma_s \text{ at } t_k \\ \hat{T}_f^n = T_s^n & \text{on } \Gamma_f \text{ at } t_c \end{cases} \quad (12)$$

Consequently, the Robin condition applied to the solid solver becomes:

$$\hat{q}_s^n = -inter_t(q_f^{n-1}) + \alpha_f^{n-1} (T_s^{n-1} - \hat{T}_s^n) \quad \text{on } \Gamma_s \text{ at } t_k \quad (13)$$

where the new relaxation term will cancel or become negligible at convergence. Indeed, the difference $(T_s^{n-1} - \hat{T}_s^n)$ is very small at convergence making the relaxation term negligible. Using this method, the solution of the coupled problem does not depend on the coupling coefficient.

2.9.3. Linear relationship between heat flux and temperature (DR3)

A linear temporal interpolation is a priori unfounded. It has been used because it is a direct and practical means to obtain solid BC when no fluid states are available. Assuming a linear variation in time of the heat flux could be a good approximation in the case of small periods of time, but in specific scenarios, such as the cruise phase in an aircraft flight, this may not be valid.

In contrast, Newton's law of cooling states that the heat flux is directly proportional to the difference in the temperatures between the body and its surroundings:

$$q = h(T - T_{ref}) \quad (14)$$

where T is the surface temperature of the body and T_{ref} is a reference temperature, usually the temperature of the surrounding fluid far from the surface.

Therefore, an other option may be to linearly interpolate the heat flux as a function of the temperature:

$$q(T(t)) = q(T(t_1)) + \frac{q(T(t_2)) - q(T(t_1))}{T(t_2) - T(t_1)} (T(t) - T(t_1)) \quad t_1 \leq t \leq t_2 \quad (15)$$

The equations characterizing this methods are:

$$\begin{cases} \hat{q}_s^n + \alpha_f^{n-1} \hat{T}_s^n = -inter_T(q_f^{n-1}) + \alpha_f^{n-1} T_s^{n-1} & \text{on } \Gamma_s \text{ at } t_k \\ \hat{T}_f^n = T_s^n & \text{on } \Gamma_f \text{ at } t_c \end{cases} \quad (16)$$

where $inter_T(q_f^{n-1})$ indicates the linear interpolation with respect of the temperature of the heat flux.

As will be shown, this relationship is more accurate than the *DR2* method but it is less robust. Indeed, the denominator in Eq. 15 ($T(t_2) - T(t_1)$) may cancel, unlike the time interpolation of the *DR2* method where the time is a growing function (i.e. $t_2 > t_1$). It is important to emphasize that Newton's law (Eq. 14) is valid with small temperature differences ($T_w - T_{ref}$) and for a constant reference temperature T_{ref} , as Davidzon (2012) has shown. If the reference temperature varies in time, it is necessary to take into account also this variation. In this case, the heat flux is linearly dependent on the difference ($T(t) - T_{ref}(t)$). For simplicity sake, $T(t_x)$ will be typed as T_x , as well as $q(T(t_x)) \Rightarrow q_x$ and $T_{ref}(x) \Rightarrow T_{refx}$, where $x = 1, 2$. The linear relationship becomes:

$$q(t) = f(T_w(t) - T_{ref}(t)) \quad (17)$$

$$q(t) = \frac{(q_2 - q_1)[T(t) - T_{ref}(t)] + (T_2 - T_{ref2})q_1 - (T_1 - T_{ref1})q_2}{T_2 - T_{ref2} + T_{ref1} - T_1} \quad (18)$$

Note that for a constant reference temperature Eq. 18 becomes Eq. 15.

2.9.4. Reference solution (*DR0*)

The previous methods have been compared to a reference solution, named *DR0*. This solution has been obtained by coupling the fluid and solid problem systematically at very solid physical time step. This means that no interpolation of the fluid states is needed, i.e. a steady CFD calculation is carried out at every solid increment in time. The solid time step has been chosen in such a way to have the mesh Fourier number $D_s \approx 0.5$ correspond to the stability criterion for explicit timestepping in one dimension. Using this value the thermal transfer is stable and a high-resolution of the transient heat conduction in the solid is obtained.

2.9.5. Summary of the methods

Table 2 summarizes the main features of the methods just described. Information is included to highlight the difference between the methods requiring the interpolation of the available fluid states (*DR1*, *DR2*, *DR3*). The

reference solution (DR0) needs no interpolation, and therefore no relaxation (Neumann condition) should be used to ensure the conservativity on the fluid-solid interface.

Method	Δt_c	Sub-iterations	q_f^{n-1}	α_f^{n-1}	T_f^{n-1}
DR0	Δt_s	No	q_f^{n-1}	0.	-
DR1	Δt_c	Yes	$inter_t(q_f^{n-1})$	$\forall \alpha_f^{n-1} \in \mathbb{R}^+$	$inter_t(T_f^{n-1})$
DR2	Δt_c	Yes	$inter_t(q_f^{n-1})$	$\forall \alpha_f^{n-1} \in \mathbb{R}^+$	T_s^{n-1}
DR3	Δt_c	Yes	$inter_T(q_f^{n-1})$	$\forall \alpha_f^{n-1} \in \mathbb{R}^+$	T_s^{n-1}

Table 2: Summary of the characteristics of the methods

In the case of the other methods it is necessary to use an iterative method; the coupling problem should then theoretically converge to the same solution for all values of the coupling coefficient.

2.10. Improving the accuracy of the Dirichlet-Robin interface treatment

In practical applications, coupling problems are usually solved by transferring quantities at the cell center of both fluid and solid faces. For the fluid domain, usually solved with the FVM, the cell center is the best location to send and receive information. However, for the solid domain, where the FEM is used, the cell center is not a good choice because neither the temperature nor the heat flux are evaluated there. Indeed, in the FEM, since the Robin condition combines temperature (Dirichlet condition) and heat flux (Neumann condition), it is necessary to evaluate the integral on the boundary where it is applied. This integral is computed using a quadrature method that approximates the definite integral of the function, usually stated as a weighted sum of function values at specified points within the domain of integration. In FEM, they are usually the Gauss points, and, only using these n points, the quadrature can provide the exact result for polynomials of degree $2n - 1$ or less (Ern and Guermond (2004)). To increase the precision of the coupling process, it is then essential to have the values of the quantities at the integration points. In a few words, all quantities used in Section 2.9 should be evaluated at the Gauss points. This is valid for any quadrature method using its own integration points.

2.11. Importance of the high solid mesh resolution

In a coupling system, the precision and the stability of the computation depend on the level of accuracy in each code. While refining the fluid mesh at the wall for a good boundary layer resolution is a common practice, this is far from being the case in the solid domain. It is generally agreed that, as thermal conduction is linear, a first order coarse mesh can provide a meaningful estimation of the temperature field. However, in transient thermal analysis, where it is possible to encounter locally large thermal gradients, this estimation may not be sufficiently accurate. This inaccuracy may affect the precision of the coupled problem solution. The coupled problem is solved through an iterative process in which the solution error may grow over time, i.e. a part of the information is lost at each transfer. It is essential to bear in mind that the heat flux is a quantity derived from the temperature field, resulting in an order of resolution lower than the temperature. In thermal analysis, a first-order mesh is generally used in the solid domain, so the heat flux in each direction is constant in the cell. This is not adequate for large temperature gradients. This can be particularly devastating if a solid heat flux (Robin condition) is applied on the fluid side. Indeed, the fluid problem will converge to another solution computed with the averaged heat flux sent by the solid solver. Therefore, the coupled problem will converge to a solution different from the real solution, without any suspicion from the user. In test case section, a clear example will be shown. To remedy this situation it is necessary to refine the solid mesh near the interface and/or use a high-order resolution of the solid problem.

3. Test case

In this section a comparison between the DR1, DR2, DR3 numerical schemes is provided through a simple test case with strong aerothermal coupling, employing DR0 as a reference computation solution.

3.1. Test case description

The test configuration is a 2D flat plate with dimensions of $350mm$ (length) \times $3mm$ (thickness). The plate is preceded by a $150mm$ long "buffer zone" with an adiabatic wall condition (see Figure 4), which provides coherent conditions at the leading edge of the plate (at $x = 0$), computed from the inlet flow (at $x = -150mm$).

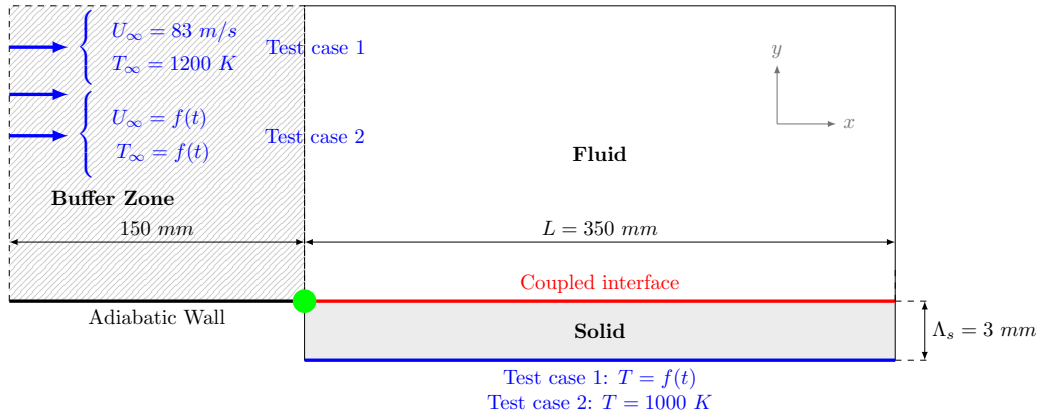


Figure 4: Flat plate with upstream buffer zone. Operating conditions for the two test cases. The green circle highlights the leading edge of the flat plate.

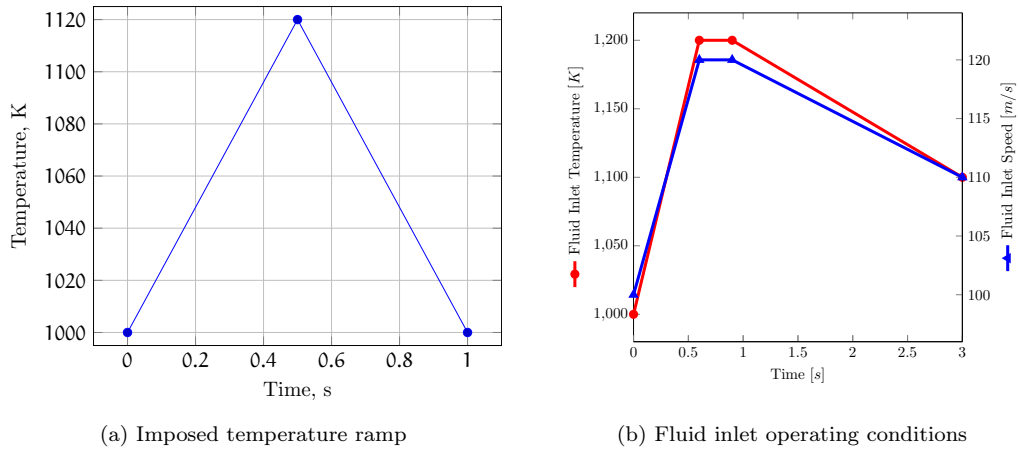


Figure 5: Unsteady conditions for the two configurations

This physical test configuration will be used for two sets of comparisons on the various numerical schemes defined above. Unsteadiness can come from either:

1. a temperature ramp on the underside of the solid plate (see Fig. 5a);
or
2. temperature and velocity ramps on the inlet flow (see Fig. 5b).

In Figure 4, the boundary conditions for the two set of comparisons are illustrated.

The aim of this study is not to provide optimal coefficients at the fluid-solid interface (see Errera et al. (2017) and the summary in Section 2.7) but to show how the traditional schemes, based on various α_f , can lead to large discrepancies.

At this point, two topics are now emphasized:

- solution-independency with respect to the coupling coefficient.
- space location of the interfacial quantities on the solid domain.

The precision metric will be based on the computed time-wise profiles of temperature and heat flux, comparing first between $\alpha = 0.$ and $\alpha = 1.e5$, and second with the reference solution provided by the (costly) DR0 scheme, which does not use time interpolation since each computed point is a coupling point. Comparisons will be made here on the upper surface of the plate, at its leading edge (green circle in Fig. 4), using the Dirichlet-Robin boundary condition.

Notice that the leading edge of the plate, at the limit between the adiabatic wall and the coupling interface, is a singular point for the thermal problem; in its neighborhood the heat flux reaches the highest values of this test case, with a very steep gradient, see Fig. 6. Consequently, this region is critical (stiff initialization of parabolic problem) for aerothermal coupling.

3.2. Numerical tools

Three numerical tools are used for the numerical solution of the coupled aerothermal problem:

- elsA (ONERA-Airbus-Safran property), a FVM solver, for the CFD problem (Cambier and Gazaix (2002); Cambier et al. (2013));

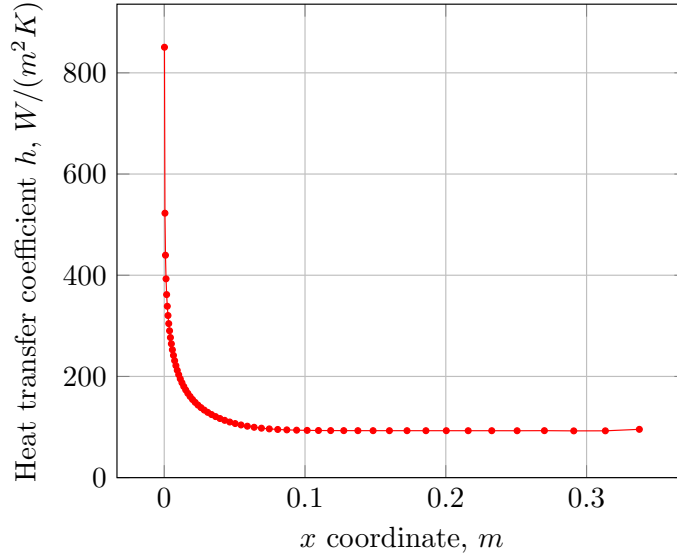


Figure 6: Heat transfer profile h along the coupled interface

- Z-set/Zébulon, a FEM solver, for the thermal problem in the solid plate (Zset-software (2018));
- CWIPI, a coupling library, for the space-interpolation between the solid and fluid meshes (CWIPI (2018)).

3.3. Numerical parameters

The mesh on both the solid and the fluid sides must be considerably refined in the x (stream flow) direction at the leading edge of the plate, to ensure a good representation of the high values of the h transfer coefficient in this region, as illustrated in Fig. 6. The first mesh cell size in the x -direction has thus been set at 0.33 mm . The solid mesh in the y direction (normal to the plate) is generated using 10 points, for a minimal mesh size of 0.33 mm . In this study, the turbulence is modeled with the Reynolds-Averaged Navier-Stokes (RANS) approach with the Spalart-Allmaras model. The fluid mesh near the wall has been refined enough to have the dimensionless wall distance near the unit ($y^+ \approx 1$). This feature allows to solve accurately the boundary layer without needing a wall law. Figure 7 shows the mesh refinement near the leading edge. Matching meshes at the coupled interface are used.

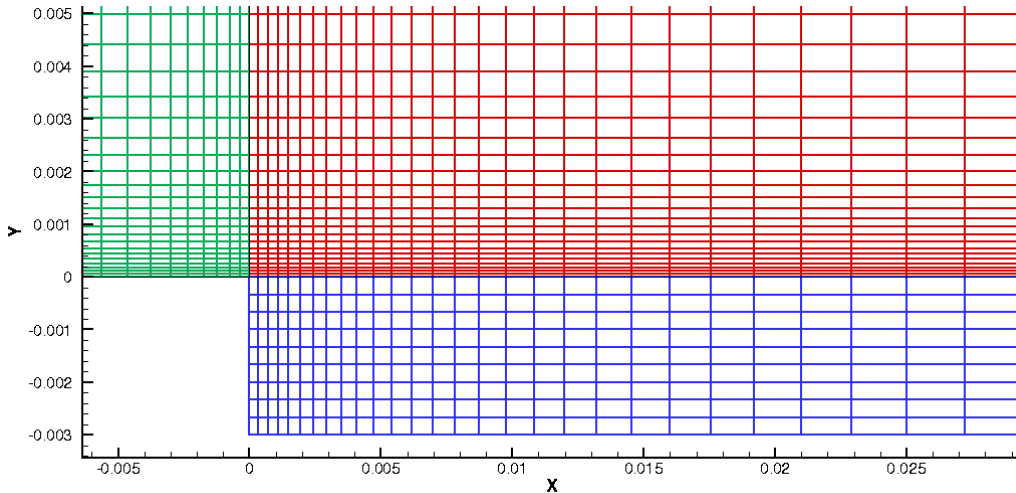


Figure 7: Solid (blue area) and fluid meshes (the buffer zone is green and the fluid coupled domain is in red) near the leading edge (the unit of length is the meter, with different scales for the x and y axes).

The coupling instants (except for the DR0 scheme) are chosen as the defining points of the temperature ramp. Convergence of the coupling is defined as $\Delta T \leq 10^{-3}$, where $\Delta T = \|T_s^n - T_s^{n-1}\|$, computed on the coupled interface.

3.4. Test case 1: unsteadiness from a temperature ramp in the solid domain

A steady fluid flow ($U_\infty = 83 \text{ m/s}$, $T_\infty = 1200\text{K}$) is imposed on the upper side, and a transient temperature ramp $T(t)$ is imposed uniformly on the lower side (see Fig. 4). The imposed temperature starts at 1000K at $t = 0\text{s}$, raises to 1120K at $t = 0.5\text{s}$, and returns to 1000K at $t = 1\text{s}$ (see Fig. 5a). The Reynolds number Re is $2.9 \cdot 10^{-5}$ and the dimensionless wall distance $y^+ \approx 0.9$.

We will illustrate here the differences, in terms of precision, obtained with the DR1, DR2, DR3 numerical schemes, and DR0.

We will focus our attention to the leading edge of the plate (the start of the coupled interface), which is – theoretically and practically – the region where most difficulties are experienced.

3.4.1. Parameters

Table 3 summarizes the most important parameters characterizing the thermal problem.

k	ρC_p	Δy_s	Δt_s	D_s	Bi
13.6	$1.36 \cdot 10^6$	$3.3 \cdot 10^{-4}$	$1.67 \cdot 10^{-2}$	1.53	0.1

Table 3: Summary of the numerical & physical parameters for test case 1

The Biot number Bi has been chosen to be very small in order to have stable computations, even with no relaxation. Indeed, as Errera et al. (2017) show in their paper, in the case of low Biot number a computation using the Dirichlet-Robin interface condition is unconditionally stable for every value of the coupling coefficient.

3.4.2. Temperature ramp definition

The temperature distribution is a simple ramp $T(t)$ made up of linear sections, see Figure 5a, uniformly imposed to the underside of the plate (Fig. 4).

3.4.3. DR1 scheme

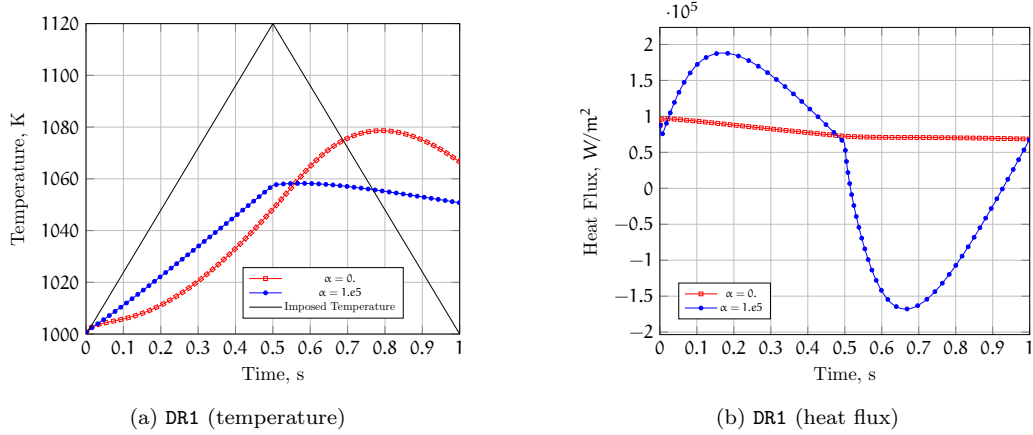


Figure 8: DR1 scheme

Figure 8 depicts a comparison of the solutions at $\alpha_f = 0.$ and $\alpha_f = 1.e5$ for the temperature and heat flux profiles at the leading edge, using the DR1 scheme based on the linear interpolation with respect to time of the temperature as in Eq. 10 (same as for the flux) defined in 2.9.1.

These Figures show that the thermal evolution in the solid domain strongly depends on the value of the coupling coefficient. This confirms the discussion of Section 2.9.1. Herein the large coupling coefficient amplifies the

relaxation term in Eq. 11, causing the linear behavior of the temperature profile. As mentioned before, the coupling coefficient should by no means affect the solution at convergence, therefore from now on this method is excluded from the final comparison with the reference solution.

Note that large values of the coupling coefficient necessarily mean large Biot numbers, i.e. a strong fluid-solid thermal interaction. In these cases a Neumann condition imposed on the fluid side should be more appropriate.

3.4.4. DR2 scheme

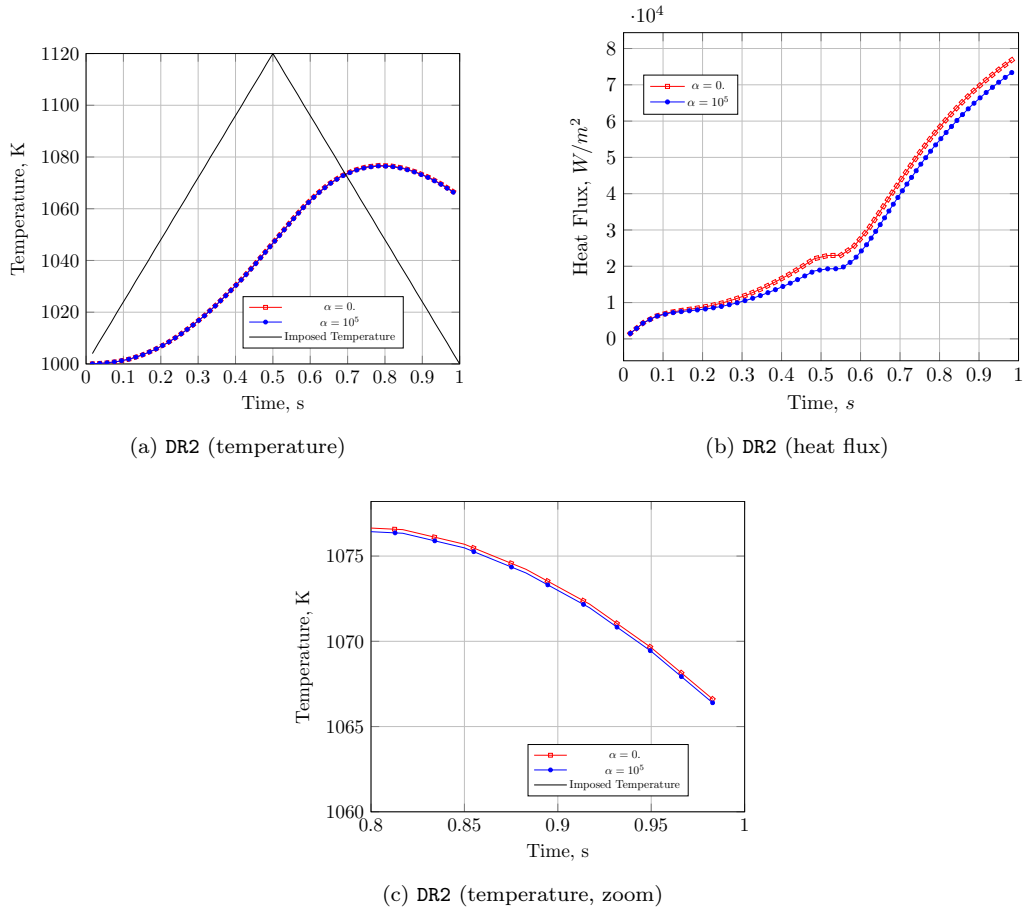


Figure 9: DR2 scheme

DR2 scheme using the element centers. Figure 9 shows that the solutions for $\alpha = 0.$ and $\alpha = 1.e5$ for the temperature and heat flux profiles at the

leading edge using the DR2 scheme. It is based on the linear interpolation with respect to time of the fluid heat flux and on the reuse of the solid temperature computed in the previous coupling iteration, as already explained in 2.9.2.

Figure 9a shows that these solutions seem very close. However, a small influence of the coupling coefficient can be noticed when examining a zoomed view of the temperature profile or the heat flux profile (see Figures 9c and 9b). The DR2 method considerably reduces the solution dependency on the coupling coefficient. The remaining difference is due to the application of the coupled quantities at the element center, which is not the most appropriate location for the Gaussian quadrature method.

DR2 scheme using the Gauss points. This section illustrates the additional precision gained applying the Robin condition quantities at the Gauss Points, i.e. the most appropriate location for the Gaussian quadrature as discussed in Section 2.10.

Figure 10 shows the solutions at $\alpha = 0.$ and $\alpha = 1.e5$ for the temperature and heat flux profiles at the leading edge, using the DR2 scheme with Gauss points, compared to the standard scheme using the element centers, as described in the previous paragraph.

The temperature profile in Figure 10a seems mostly unaffected by the various choices. The heat flux profile, on the other hand, is noticeably (about 6%) different when using Gauss points or elements, see Figures 10b, 10c. Note the minuscule difference on the heat flux, about $100 W/m^2$ (undetectable on the Figure), between the calculation using $\alpha = 0.$ (red line) and the one using both $\alpha = 10^5$ and the application at the Gauss points (green line). This is the result of the product of the coupling coefficient ($\alpha = 10^5$) and the convergence criterion on the temperature ($\Delta T \leq 10^{-3} K$). This product corresponds to the relaxation term of the Robin condition (Eq. 13), i.e. the expected error in accordance with the chosen convergence level.

DR2 scheme: influence of the y-mesh refinement. Figure 11 illustrates the influence of the y-mesh refinement on the heat flux time-wise profile in a thermal coupled problem. In this example a zero coupling coefficient is used to impose only the heat flux on the solid solver (Neumann condition). In each Figure we have plotted (1) the fluid heat flux received at the Gauss points in the solid interface before the solid computation, (2)the heat flux sent by the solid element center to the fluid after the computation, and (3)the solid heat flux computed by the solid solver at the cell center. Theoretically,

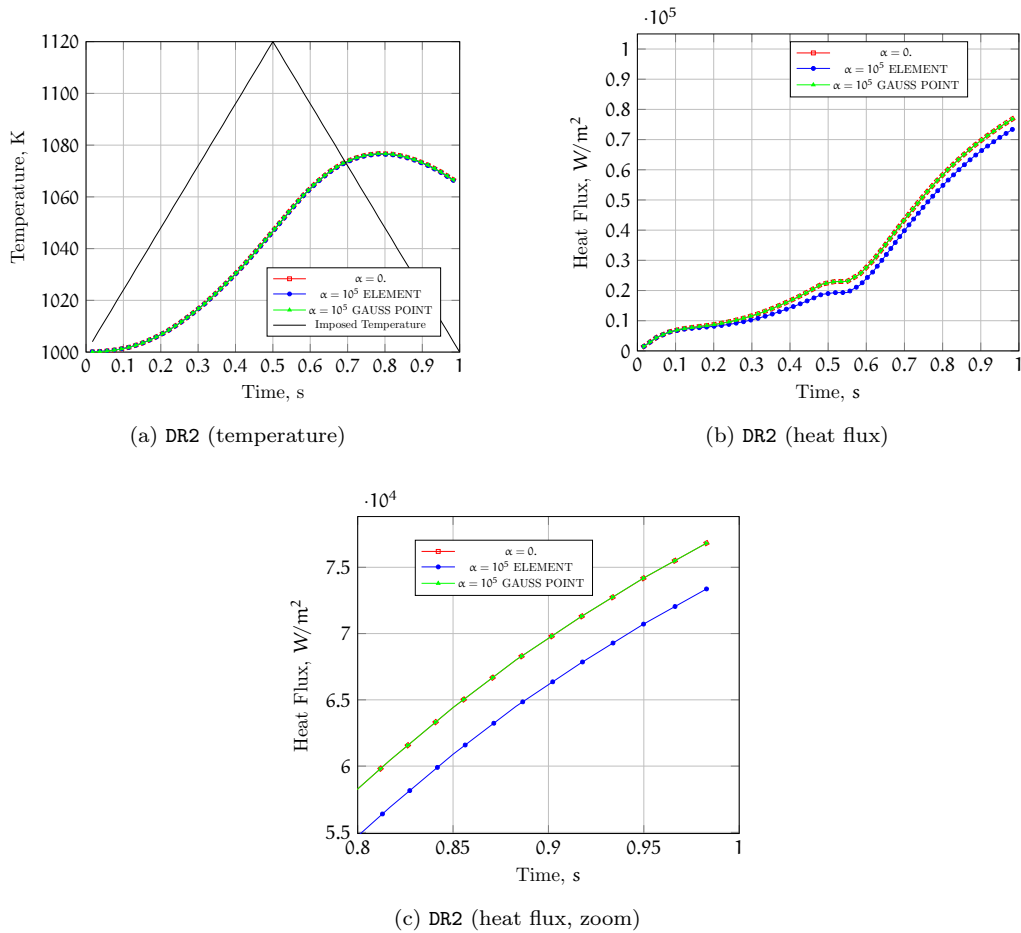


Figure 10: DR2 scheme, Gauss points vs. elements

when a Neumann condition is applied on the solid side, all these quantities are expected to be equal. Figure 11a shows that the heat flux computed by the solid solver and the one sent to the fluid are the same, i.e. the solid solver correctly sends the computed value. But there is a large difference between the heat flux received before the computation and the one sent after the computation. This discrepancy means that the solid mesh near the coupled interface is not appropriate for the level of amplitude of the thermal gradient. As explained in Section 2.11, in a FEM linear mesh cell the heat flux is constant along one direction. Indeed, the computed value of the normal heat flux (23134.8 W/m^2 in the leading edge at $t = 0.5 \text{ s}$ for example) in the first solid cell is the average of the imposed heat flux and

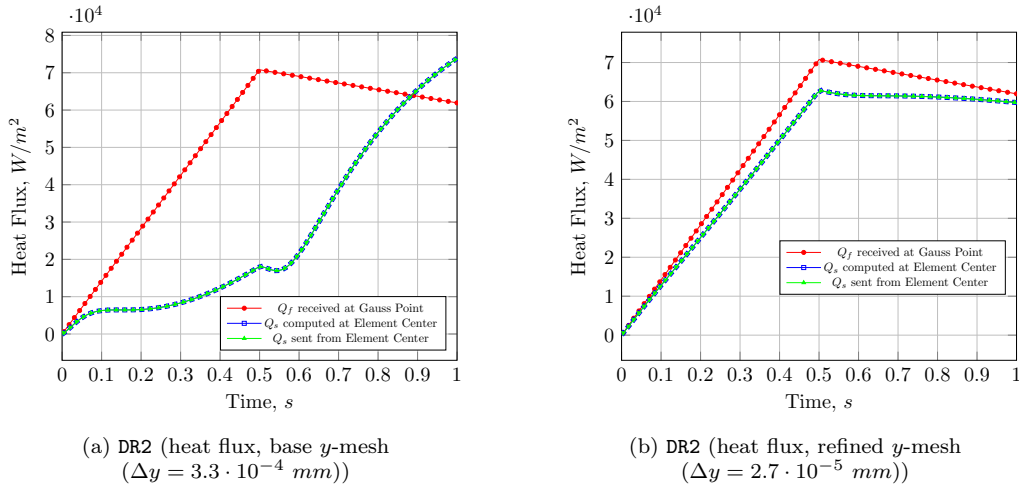


Figure 11: DR2 scheme, influence of y -mesh refinement

the one computed in the second cell (see Fig. 12). The legend of the same figure stresses the discrepancy in the heat flux for this test case: a variation of $6.745e + 05 \text{ W/m}^2$ is observed along the thickness ($2.313e + 04 \text{ W/m}^2$ at the leading edge and $-6.514e + 05 \text{ W/m}^2$ at the bottom surface of the flat plate). Obviously this large gradient in temperature cannot be well captured using only 9 cells. By refining the mesh, the resolution of the heat flux can be improved, as Figure 11b illustrates. Theoretically, it is possible to have the exact solution by making the first solid cell infinitely small. In practice, this is impossible. In addition to the mesh refinement, it may be appropriate to implement a high-order resolution of the solid problem. The use of a coarse mesh in the previous studies does not put into question the results of the coupled problem because the Dirichlet condition is used on the fluid side. The solid heat flux is not transferred in the coupling process. However, a good resolution of the heat flux would have been essential if a Neumann or Robin condition were used.

From now on, the refined mesh will be used.

3.4.5. Reference computation DR0

The DR0 reference "scheme" completely avoids the interpolation issues – for which the DR1, DR2 and DR3 schemes will be analyzed – by enforcing coupling at every time station. Moreover, a low Fourier number ($D_s = 0.5$) is used to ensure adequate precision.

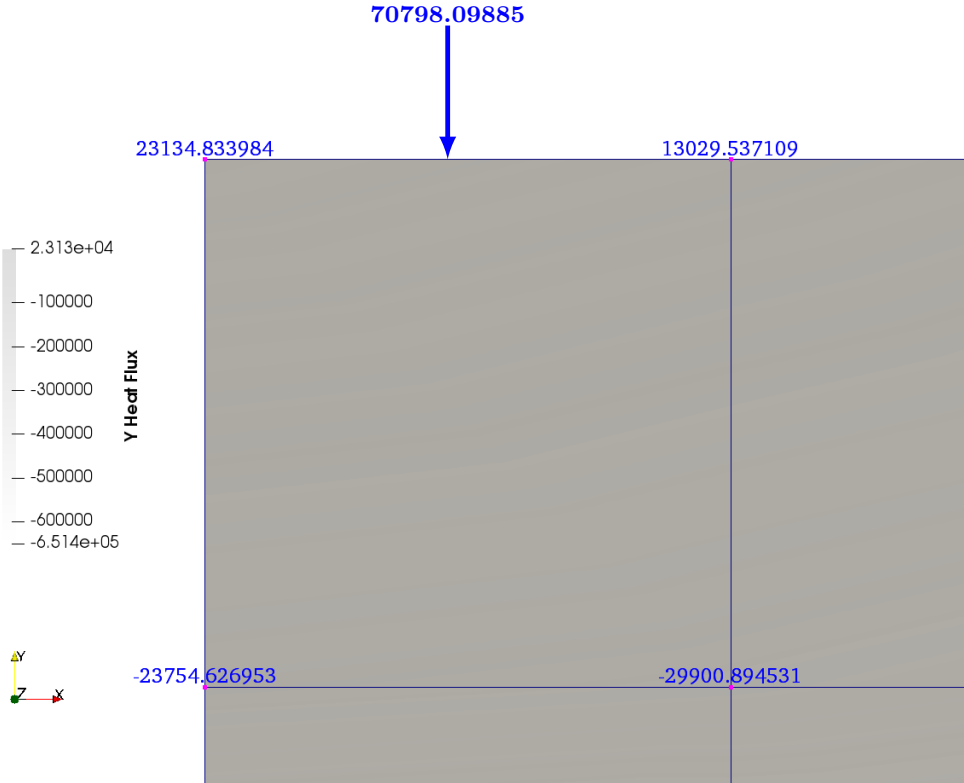


Figure 12: Heat flux field in the solid leading edge cell at $t = 0.5 \text{ s}$
 (base y -mesh ($\Delta y = 3.3 \cdot 10^{-4} \text{ mm}$))

Figure 13 depicts the temperature and heat flux time-wise profiles for this reference solution on the current test case. This will be the comparison basis for the DR1, DR2 and DR3 schemes. We have changed the initialization of the computation to facilitate the execution of the costly DR0 computation. This explains the different form of heat flux computed during this last computation compared to the previous simulations.

3.4.6. DR3 scheme, comparison with DR0 and DR2

Figure 14 shows the solutions for the temperature and heat flux profiles at the leading edge, using the DR3 “precise” scheme, compared to the DR2 and DR0 schemes. Note that all the corrections seen before (the solid boundary condition using Gauss points values and the refined mesh) are applied in these last computations.

The temperature and heat flux profiles for the DR3 and DR0 schemes are

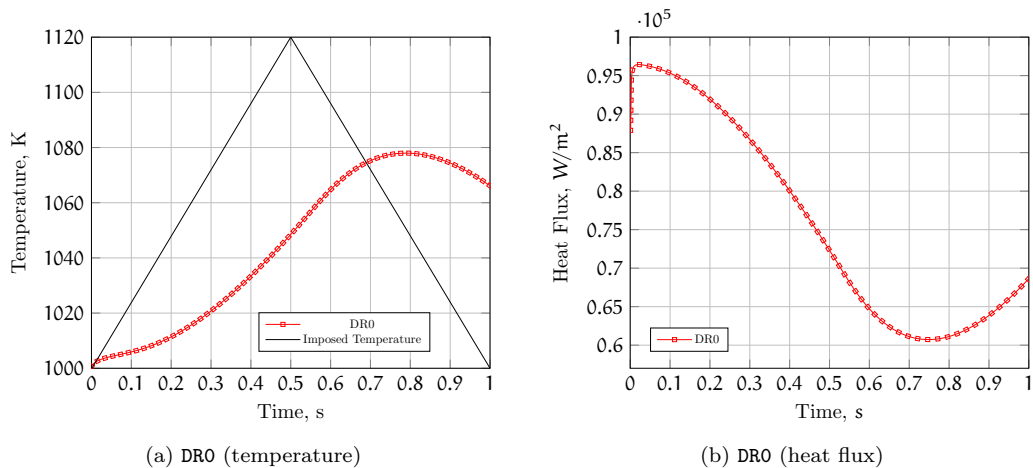


Figure 13: DR0 reference scheme

visually superimposed, see Figures 14a and 14b, whereas the DR2 scheme leads to noticeably different results, particularly in the second part of the computation. Here the temperature profile computed with the DR2 method exhibits a small difference compared with the reference and the DR3 results (see Figure 14c). The DR2 scheme imposes a time-wise linear heat flux that apparently is not appropriate. Moreover, the linear interpolation of the flux on the solid temperature (DR3 method) gives a good thermal behavior of the coupled system.

	Temperature	Heat Flux
DR2	0.062%	16.06%
DR3	0.0008%	0.13%

Table 4: Accuracy error for test case 1

Table 4 provides the percent error of the DR2 and DR3 methods compared to the reference solution DR0. The DR3 results are two orders of amplitude more accurate than the DR2 method on both temperature and heat flux fields.

3.5. Test case 2: unsteadiness from temperature and velocity ramps on the inlet flow

This section illustrates the comparison of the different methods on the same flat plate meshes shown in the previous test case section, this time using a time variation of the fluid inlet conditions and a constant temperature on the bottom surface of the solid, as shown in Fig. 4.

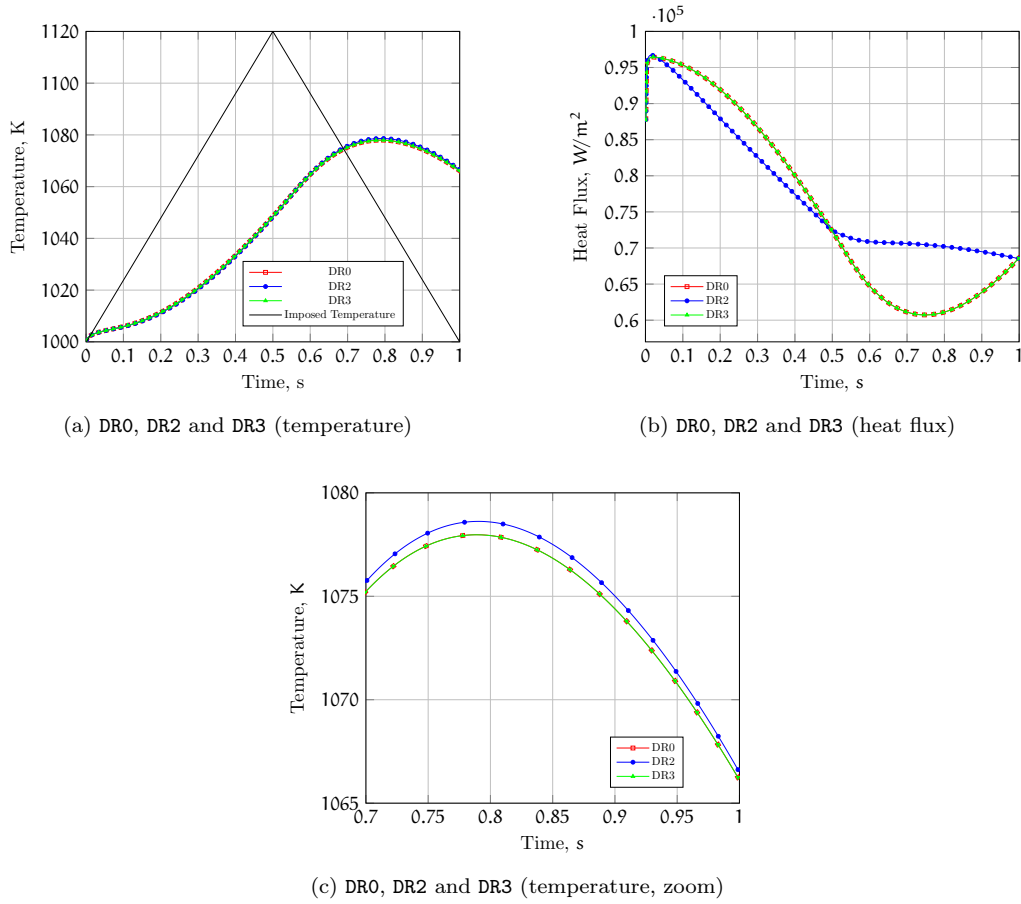


Figure 14: DR3 scheme, comparison with DR2 and DR0

3.5.1. Inlet conditions

Since only steady CFD computations are carried out, the inlet conditions will be different between coupling times. These are indicated by the markers in Fig. 5b. A time variation of both temperature and velocity at the fluid inlet is imposed.

For the reference computation (*DR0*) it is necessary to change the fluid conditions at every solid time step, so a linear interpolation of the operating conditions, used for the other methods, is applied (solid lines in Figure 5b). The Reynolds number value Re ranges between $3.6 \cdot 10^{-5}$ and $4.3 \cdot 10^{-5}$ according to the fluid inlet conditions. The dimensionless wall distance is $y^+ \approx 0.9$.

3.5.2. Parameters

The main parameters used for this case test are summarized in Table 5. They have been chosen to obtain a Fourier number close to 0.5 and a Biot number large enough to show that the proposed methods are effective even when the fluid-solid thermal interaction is strong.

k	ρC_p	Δy_s	Δt_s	D_s	Bi
0.1	$1.7 \cdot 10^6$	$2.7 \cdot 10^{-5}$	0.006	0.48	17.1

Table 5: Summary table of the important parameters for test case 2

3.5.3. Results

Figure 15 depicts the solution for the temperature and the heat flux profiles at the leading edge, using the *DR2* and *DR3* methods, compared to the reference computation *DR0*.

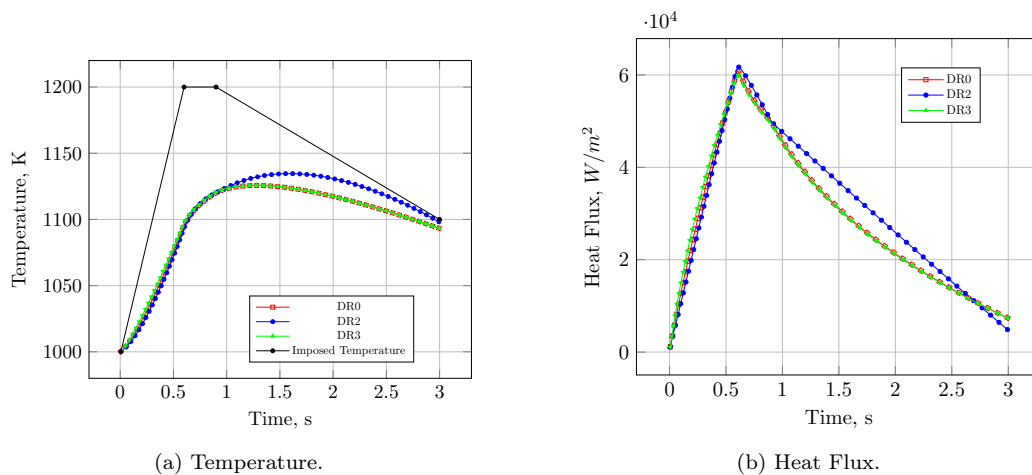


Figure 15: 3 scheme, comparison with 2 and 0

The temperature profile is represented in Figure 15a. Clearly, the *DR2* method produces large discrepancies after the second coupling instants ($t = 0.9$) when the heat flux is not linear anymore, as we can see in Fig. 15b. Indeed, *DR2* and *DR3* closely follow the temperature profile of the reference computation while the heat flux displays linear behavior, which is in turn due to a large temperature gradient from the fluid inlet. But once the gradient generated by the fluid inlet decreases, only *DR3*, which uses a

linear interpolation between heat flux and temperature defining in Eq. 17, demonstrates a very good behavior through the whole temporal process.

	Temperature	Heat Flux
DR2	1.21%	35.65%
DR3	0.36%	19.69%

Table 6: Accuracy error for test case 2

Table 6 shows the percent error for this last test case. This time the error is larger than the one in the previous test case. This confirms that considering the fluid as a sequence of steady states is not a very accurate approximation when a strong unsteadiness comes from the fluid flow. The DR3 method produces more accurate results than those of the DR2 method.

4. Conclusion

In a flight cycle, the solid calculations in the CHT process must be unsteady in order to analyze the "slow" response of the metal heat conduction to the changing of loading conditions of the engine, while a "fast" fluid convection is adopted. This is the first simplifying assumption in the quasi-dynamic procedure, imposed at ramp points, where environmental parameters are defined. Furthermore, as a further approximation, between two end points of a ramp, the transient solid solution is obtained with interpolated boundary conditions estimated by a linear interpolation. In this paper, a CHT reference computation not based on these two assumptions has been carried out in order to assess and to improve the accuracy of the basic procedures.

First, as expected, it has been demonstrated that a temporal interpolation is not the most appropriate way of estimating the flow boundary conditions. Indeed, this approximation seems unfounded in most situations and can lead to serious temporal inaccuracies. On the contrary, on the basis of Newton's law of cooling, the heat flux can be estimated as a linear function of the temperature. This remains an approximation, but all the results presented in this paper show that this physics-based relationship yields significantly better results. This is key point since the interpolation method between two ramp points has a significant impact on the temporal prediction of metal temperatures

Second, it has been shown that a little inaccuracy on the temperature estimation may lead to inconsistent results. A larger Biot number leads to

greater inaccuracy in estimation. It then becomes fundamental to properly define the integral contribution of the boundary condition using the values at the Gauss points in the FEM solid code instead of the value at the cell centers of the faces. This point is rarely mentioned in the CHT literature.

Moreover, it is important to note that particular attention should be paid to sufficient refinement of the solid mesh in order to have a good evaluation of the solid heat flux. This is all the more important since a finite-element solid solver is used.

Finally, it is worth noting that, as expected, the influence of the fluid unsteadiness is negligible for a ramp representing steady flight conditions (idle, cruise conditions). However, in the case of a sudden acceleration or deceleration, results obtained with a steady CFD model are questionable. However, this was not the main objective of this paper and other tests involving sudden rapid changes in the flow domain are needed.

As a general conclusion it appears that the simulation results, based on the interpolation procedures proposed in this paper, compare very well against a reference solution computed with a method using no interpolation.

Acknowledgments

The authors would like to acknowledge the Direction Scientifique Générale de l'ONERA for their support. The studies presented in this article make use of elsA-ONERA, a software package jointly owned by Airbus, Safran, and ONERA. Thanks also to Minh Nguyen for his re-reading of this article.

References

References

- Amirante, D., Hills, N. J., Barnes, C. J., 2012. Thermo-mechanical finite element analysis/computational fluid dynamics coupling of an interstage seal cavity using torsional spring analogy. *Journal of Turbomachinery* 134 (5), 051015.
URL <http://Turbomachinery.asmedigitalcollection.asme.org/article.aspx?articleid=1485156>
- Baque, B., Errera, M.-P., Roos, A., Feyel, F., 2013. Simulation of transient conjugate heat transfer via a temporal multiscale approach. *International Journal for Multiscale Computational Engineering* 11 (4), 333–345.

- URL <http://www.dl.begellhouse.com/journals/61fd1b191cf7e96f,0166231359bf4331,72650fb32ce515c3.html>
- Cambier, L., Gazaix, M., Jan. 2002. *elsA* - An efficient object-oriented solution to CFD complexity. In: 40th AIAA Aerospace Sciences Meeting & Exhibit. Aerospace Sciences Meetings. American Institute of Aeronautics and Astronautics.
URL <https://doi.org/10.2514/6.2002-108>
- Cambier, L., Heib, S., Plot, S., 2013. The Onera *elsA* CFD software: input from research and feedback from industry. *Mechanics & Industry* 14 (3), 159–174.
URL <http://www.mechanics-industry.org/10.1051/meca/2013056>
- CWIPI, 2018. La bibliothèque de couplage CWIPI | Coupling With Interpolation Parallel Interface.
URL <https://w3.onera.fr/cwipi/>
- Davidzon, M. I., Oct. 2012. Newton’s law of cooling and its interpretation. *International Journal of Heat and Mass Transfer* 55 (21-22), 5397–5402.
URL <http://linkinghub.elsevier.com/retrieve/pii/S0017931012001846>
- El Khoury, R. R., Errera, M., El Khoury, K., Nemer, M., May 2017. Efficiency of coupling schemes for the treatment of steady state fluid-structure thermal interactions. *International Journal of Thermal Sciences* 115 (Supplement C), 225–235.
URL <http://www.sciencedirect.com/science/article/pii/S1290072916306548>
- Ern, A., Guermond, J., 2004. *Theory and practice of finite elements*. Applied Mathematical Sciences. Springer New York.
URL <https://books.google.fr/books?id=CCjm79FbJbcC>
- Errera, M.-P., Baqué, B., Aug. 2013. A quasi-dynamic procedure for coupled thermal simulations. *International Journal for Numerical Methods in Fluids* 72 (11), 1183–1206.
URL <http://doi.wiley.com/10.1002/flid.3782>
- Errera, M.-P., Chemin, S., Jul. 2013. Optimal solutions of numerical interface conditions in fluid–structure thermal analysis. *Journal of Computational*

- Physics 245 (Supplement C), 431–455.
 URL <http://www.sciencedirect.com/science/article/pii/S0021999113001770>
- Errera, M.-P., Duchaine, F., May 2016. Comparative study of coupling coefficients in Dirichlet–Robin procedure for fluid–structure aerothermal simulations. *Journal of Computational Physics* 312 (Supplement C), 218–234.
 URL <http://www.sciencedirect.com/science/article/pii/S0021999116000760>
- Errera, M.-P., Lazareff, M., Garaud, J.-D., Soubrié, T., Douta, C., Federici, T., Jul. 2017. A coupling approach to modeling heat transfer during a full transient flight cycle. *International Journal of Heat and Mass Transfer* 110, 587–605.
 URL <http://linkinghub.elsevier.com/retrieve/pii/S0017931016331222>
- Errera, M.-P., Turpin, G., Apr. 2013. Temporal multiscale strategies for conjugate heat transfer problems. *Journal of Coupled Systems and Multiscale Dynamics* 1 (1), 89–98.
 URL <http://openurl.ingenta.com/content/xref?genre=article&issn=2330-152X&volume=1&issue=1&spage=89>
- Farhat, C., Lesoinne, M., 2000. Two efficient staggered algorithms for the serial and parallel solution of three-dimensional nonlinear transient aeroelastic problems. *Comput. Methods Appl. Mech. Engrg.*, 17.
- Felippa, C. A., Park, K. C., 1980. Staggered transient analysis procedures for coupled mechanical systems: formulation. *Computer Methods in Applied Mechanics and Engineering* 24 (1), 61–111.
- Ganine, V., Javiya, U., Hills, N., Chew, J., 2012. Coupled fluid-structure transient thermal analysis of a gas turbine internal air system with multiple cavities. *Journal of Engineering for Gas Turbines and Power* 134 (10), 102508.
 URL <http://GasTurbinesPower.asmedigitalcollection.asme.org/article.aspx?articleid=1477085>
- Gimenez, G., Errera, M., Baillis, D., Smith, Y., Pardo, F., Jun. 2016. A coupling numerical methodology for weakly transient conjugate heat transfer

- problems. *International Journal of Heat and Mass Transfer* 97, 975–989.
URL <http://linkinghub.elsevier.com/retrieve/pii/S0017931015304385>
- He, L., Fadl, M., Apr. 2017. Multi-scale time integration for transient conjugate heat transfer: Multi-scale Time Integration for Transient Conjugate Heat Transfer. *International Journal for Numerical Methods in Fluids* 83 (12), 887–904.
URL <http://doi.wiley.com/10.1002/flid.4295>
- He, L., Oldfield, M. L. G., 2009. Unsteady conjugate heat transfer modelling. ASME, pp. 101–114.
URL <http://proceedings.asmedigitalcollection.asme.org/proceeding.aspx?articleid=1646820>
- Henshaw, W. D., Chand, K. K., Jun. 2009. A composite grid solver for conjugate heat transfer in fluid–structure systems. *Journal of Computational Physics* 228 (10), 3708–3741.
URL <http://linkinghub.elsevier.com/retrieve/pii/S0021999109000667>
- Jaiman, R., Jiao, X., Geubelle, P., Loth, E., Oct. 2006. Conservative load transfer along curved fluid–solid interface with non-matching meshes. *Journal of Computational Physics* 218 (1), 372–397.
URL <http://linkinghub.elsevier.com/retrieve/pii/S0021999106000891>
- Jaiman, R. K., Jiao, X., Geubelle, P. H., Loth, E., Dec. 2005. Assessment of conservative load transfer for fluid-solid interface with non-matching meshes. *International Journal for Numerical Methods in Engineering* 64 (15), 2014–2038.
URL <http://doi.wiley.com/10.1002/nme.1434>
- Jiao, X., Heath, M. T., Dec. 2004. Common-refinement-based data transfer between non-matching meshes in multiphysics simulations. *International Journal for Numerical Methods in Engineering* 61 (14), 2402–2427.
URL <http://doi.wiley.com/10.1002/nme.1147>
- Joshi, O., Leyland, P., Jan. 2014. Stability analysis of a partitioned fluid–structure thermal coupling algorithm. *Journal of Thermophysics and Heat Transfer* 28 (1), 59–67.
URL <http://arc.aiaa.org/doi/10.2514/1.T4032>

- Kazemi-Kamyab, V., van Zuijlen, A. H., Bijl, H., 2014. Accuracy and stability analysis of a second-order time-accurate loosely coupled partitioned algorithm for transient conjugate heat transfer problems. *International Journal for Numerical Methods in Fluids* 74 (2), 113–133.
URL <http://dx.doi.org/10.1002/flid.3842>
- Koren, C., Vicquelin, R., Gicquel, O., Aug. 2017. Self-adaptive coupling frequency for unsteady coupled conjugate heat transfer simulations. *International Journal of Thermal Sciences* 118, 340–354.
URL <https://linkinghub.elsevier.com/retrieve/pii/S1290072916305932>
- Kuntz, D. W., Hassan, B., Potter, D. L., Apr. 2001. Predictions of ablating hypersonic vehicles using an iterative coupled fluid/thermal approach. *Journal of Thermophysics and Heat Transfer* 15 (2), 129–139.
URL <http://arc.aiaa.org/doi/10.2514/2.6594>
- Lindström, J., Nordström, J., Jul. 2010. A stable and high-order accurate conjugate heat transfer problem. *Journal of Computational Physics* 229 (14), 5440–5456.
URL <http://linkinghub.elsevier.com/retrieve/pii/S0021999110001865>
- Liu, Q., Luke, E. A., Cinnella, P., Oct. 2005. Coupling heat transfer and fluid flow solvers for multidisciplinary simulations. *Journal of Thermophysics and Heat Transfer* 19 (4), 417–427.
URL <http://arc.aiaa.org/doi/10.2514/1.13522>
- Moretti, R., Errera, M.-P., Couaillier, V., Feyel, F., Apr. 2018. Stability, convergence and optimization of interface treatments in weak and strong thermal fluid-structure interaction. *International Journal of Thermal Sciences* 126, 23–37.
URL <https://www.sciencedirect.com/science/article/pii/S1290072917308785>
- Mukherji, B. S., K, R., Naresh, G., Rao, V. N. B., Kumar, I. N. a., Dec. 2015. An investigation of transient thermal analysis of 1st stage gas turbine blade manufactured by directional solidification and mechanically alloyed nickel-based superalloys. *International Journal of Advanced Science and Technology* 85, 17–28.
URL <http://www.sersc.org/journals/IJAST/vol85/3.pdf>

- Perelman, T., Dec. 1961. On conjugated problems of heat transfer. *International Journal of Heat and Mass Transfer* 3 (4), 293–303.
URL <http://www.sciencedirect.com/science/article/pii/0017931061900448>
- Piperno, S., Farhat, C., Larrouturou, B., 1995. Partitioned procedures for the transient solution of coupled aeroelastic problems Part I: Model problem, theory and two-dimensional application. *Computer methods in applied mechanics and engineering* 124 (1-2), 79–112.
- Rezazadeh Reyhani, M., Alizadeh, M., Fathi, A., Khaledi, H., Jun. 2013. Turbine blade temperature calculation and life estimation - a sensitivity analysis. *Propulsion and Power Research* 2 (2), 148–161.
URL <http://linkinghub.elsevier.com/retrieve/pii/S2212540X13000199>
- Roe, B., Jaiman, R., Haselbacher, A., Geubelle, P. H., May 2008. Combined interface boundary condition method for coupled thermal simulations. *International Journal for Numerical Methods in Fluids* 57 (3), 329–354.
URL <http://doi.wiley.com/10.1002/flid.1637>
- Sun, Z., Chew, J. W., Hills, N. J., Lewis, L., Mabilat, C., Jan. 2012. Coupled aerothermomechanical simulation for a turbine disk through a full transient cycle. *Journal of Turbomachinery*.
- Sun, Z., Chew, J. W., Hills, N. J., Volkov, K. N., Barnes, C. J., 2008. Efficient FEA/CFD thermal coupling for engineering applications. *ASME*, pp. 1505–1515.
URL <http://proceedings.asmedigitalcollection.asme.org/proceeding.aspx?articleid=1624545>
- Verstraete, T., Scholl, S., Oct. 2016. Stability analysis of partitioned methods for predicting conjugate heat transfer. *International Journal of Heat and Mass Transfer* 101 (Supplement C), 852–869.
URL <http://www.sciencedirect.com/science/article/pii/S001793101531245X>
- Zset-software, 2018. Z-set | Non-linear material & structure analysis suite.
URL <http://www.zset-software.com/>